15

Simulation of thermally induced deformations of silicon mirrors of synchrotron radiation sources

© V.S. Naumkin,[1,2] M.V. Gorbachev[2]

[1]Kutateladze Institute of Thermophysics, Siberian Branch, Russian Academy of Sciences,
630090 Novosibirsk, Russia
[2]Novosibirsk State Technical University,
630073 Novosibirsk, Russia
e-mail: vsnaumkin@itp.nsc.ru

Received November 12, 2024
Revised June 3, 2025
Accepted June 5, 2025

The results of numerical modeling of the thermally deformed state of a silicon mirror reflecting a synchrotron radiation beam are presented. It is shown that when estimating temperature fields at low coolant flow rates (low heat transfer coefficients), it is necessary to take into account the effect of the radiator. It is shown that under the studied conditions, a smart-cut under the cooling radiator can reduce the magnitude of absolute deformations by almost an order of magnitude, compared to a mirror without one. The results can be useful in designing multilayer mirror optics at undulator stations of new sources such as MAX IV, ESRF EBS, and the SKIF „Center for Collective Use".

Keywords: numerical simulation, high heat flux densities, strained state, cooling of synchrotron equipment.

DOI: 10.61011/TP.2025.10.62096.418-24

Introduction

Due to increasing power density of synchrotron radiation (SR) sources (within $1-10\,W/mm^2$), it is necessary to ensure effective cooling of optical components (mirrors, optical filters, monochromators, etc.), which are exposed to high-density radiation. Heat flux approximately equal to 1 kW may be supplied to $1\,cm^2$ of the mirror. Such high heat flux density may induce local overheating or large temperature gradients resulting in considerable surface strains of the cooled component. Thus, it is necessary to provide effective removal of the concentrated heat flux from the surface or internal volume of such mirrors.

To reduce the absolute thermally induced strains, the literature proposes mirrors with various shapes and cooling methods. Mirror shapes reported in the literature are shown schematically in Table 1. For all mirrors, SR falls from above. Cooling in all cases, except for the third one, can be provided from the bottom or top walls or from sides. In the third case, additional cooling is provided via channels passing inside the mirror. In the eighth case, the radiator is highlighted in blue.

A synchrotron flux can strike the center of the mirror surface as well as strips to the left and right of the center, therefore mirrors with previously curved surface (drawings 4 and 5) that is distorted after heating cannot ensure the necessary level of thermally induced strains during asymmetric heating. Internally cooled mirrors (drawing 3) are more dificult in manufacturing than externally cooled ones, though they, according to the literature, provide lower strains. Internal stresses in a mirror with side cooling (covering a part of the length) and cooling via internal channels were addressed in [1]. It was shown that maximum temperatures and thermally induced strains were lower with internal-channel cooling (by 40 % with respect to the maximum temperature and approximately by 4 % with respect to strains) compared with side cooling. In [2] , a mirror configuration with internal water cooling is proposed to provide a lower level of thermally induced strains than side or bottom cooling. The mirror surface is a multilayer coating consisting of a combination of tungsten and carbon.

A streamlined cooling system for a mirror reflecting laser light was described in [3]. Direct mirror cooling systems were also reviewed. It was shown that the lowest thermally induced strains were observed for channel configurations inside the mirror at 90° from the irradiated zone, moreover, the mirror also had a small concavity, which reduced the mirror thickness under the irradiated zone.

Smart-cut in the mirror, that could be made more easily than internal cooling, were proposed in [4]. In [5], the effect of side grooves in the mirror on the thermally induced strain level was discussed and side and bottom cooling effects were compared. The authors [5] made the following conclusions from their analysis:

1) side cooling of a mirror induces lower strains of the reflecting surface;

2) the higher the mirror the lower the thermally induced strain;

3) a groove can considerable reduce thermally induced strains.

Notwithstanding that mirrors with side grooves are relatively popular, there are virtually no literature data concern-

Table 1. Silicon mirror shapes

1	2	3	4	5	6	7	8
		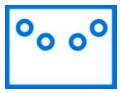					
[1], [8], [9], [5], [10], [11], [12], [13], [14], [15], [16]	[5], [4], [17]	[1], [8], [12], [2]	[18]	[2], [19]	[20]	[6]	[7]

ing systematic investigations of geometrical parameters of side grooves for the magnitude of reflecting surface strains. Therefore, one of the aims of this study is to explore the effect of side groove depth on the maximum thermally induced strains of a silicon mirror surface.

An asymmetric shape of mirror for reflection of a beam with a power density of $8\,\mathrm{W/mm^2}$ is proposed in [6]. The asymmetric mirror shape provides cooling from three directions (side, bottom and top, optionally). Water cooling with the given values of thermal input is sufficient to ensure an acceptable level of thermally induced strains.

In PhD [7], a new radiator configuration was proposed for cooling a trapezoidal mirror separated into several parts and placed between the radiator ribs. In [12], typical heat transfer coefficients of the radiator are provided:

1) $\alpha = 3000\,\mathrm{W/(m^2{\cdot}K)}$ with an adequate thermal resistance between a copper radiator and cooled mirror. Corresponds to the case when the side surface of the mirror and radiator have considerable roughness and do not fit tightly to each other.

2) $\alpha = 5000\,\mathrm{W/(m^2{\cdot}K)}$ for a good thermal contact. Corresponds to well polished mirror and radiator surfaces;

3) $\alpha = 8000\,\mathrm{W/(m^2{\cdot}K)}$ for a better thermal contact. Corresponds to a thermal contact filled with an intermediate material such as indium or invar;

4) $\alpha = 18000\,\mathrm{W/(m^2{\cdot}K)}$ a heat transfer coefficient for side cooling comparable with direct cooling inside a mirror. It is achieved by increasing the contact area of the cooled surface.

B [12] a finite element method is used to show that, for a fixed mirror configuration in a general monochromator operating range, an increase in the heat transfer coefficient doesn't cause any significant reduction of thermally induced mirror surface strains.

Active mirror exposure methods are also proposed in order to reduce thermally induced strains. Thus, a mechanism where a mirror can be bent with a predefined accuracy during operation was proposed in [9].

In [21], it was shown experimentally that mirror cooling with a coolant having a cryogenic temperature considerably reduced thermally induced strains compared with water cooling. However, cryogenic temperatures involve a lot of difficulties: some materials used in optical components become brittle, thus increasing the risk of component failure during operation; complexity and high operating cost of cryochillers, etc.

In [16], various cooling options for process laser mirrors were compared: channel cooling, cooling using porous structures, jet cooling, two-phase cooling. Relative advantages and disadvantages of each of the systems were described. It was shown that some cooling systems could provide a heat transfer coefficient up to $200\,000\,\mathrm{W/(m^2{\cdot}K)}$. Table 2 gives a summary of literature data concerning the incident radiation power Q, [W]; density of heat flux striking the mirror q, $\mathrm{W/mm^2}$; mirror sizes, cooling methods and cooling fluid flow rates (Reynolds numbers, $\mathrm{Re_d}$). The analysis shows that predominantly similar mirrors are cooled using side radiators. Internal cooling is used much more rarely. Combined cooling is used very rarely. Most studies don't consider the radiator effect, only two studies provide the Reynolds numbers for coolant [8,10]. In most cases, for evaluation of temperature distribution over the mirror surface, a constant heat transfer coefficient is maintained. In the above-mentioned literature, the heat transfer coefficient varies from 1 to $7\,\mathrm{kW/(m^2{\cdot}K)}$, which corresponds to the cooling water flow rate ranging approximately from 0.03 to 0.1 kg/s (with a radiator tube diameter of 10 mm). However, as it will be shown in this work, if the copper radiator effect is not considered at low coolant flow rates, then the mirror will be cooled asymmetrically and this cannot be detected when the heat transfer coefficient is constant. Therefore the second aim of this work is to estimate the heat transfer coefficient, for which the radiator effect must be considered.

1. Description of a problem for calculation of thermally induced stresses of ceramic mirrors

This study describes a system with side-cooled mirror with side grooves as proposed in [5,17]. The highest stresses will obviously occur on a heated narrow mirror strip. Side cooling of the mirror is assumed („cooling“) (Figure 1).

Table 2. Mirror cooling methods

References	Q [W]	q [W/mm^2]	Mirror dimensions [mm×mm×mm]	Beam dimensions on the mirror [mm × mm]	Cooling				α [kW/(m^2·K)]	Re$_d$	Coolant
					Direct (directly in crystal)	Indirect from side	Indirect from bottom	Indirect from combined			
[6]		8.5	10 × 10 × 15					×	7	–	Water
[1]	333_{max}			310.14×4.488	×	×			3	–	Water
[8]	100	0.15	40 to 150 × 25 to 35 × 40 to 70		×	×				up to 55000	Liquid nitrogen
[9]		0.0014	1200 × 120 × 58			×					–
[2]			150 × 50 × 20		×						Water
[5]	440	0.88	500 × 75 × 75	500 × 1		×	×		1		Water
[10]	1100		900 × 70 × 65	∼ 600 × ∼ 3		×				20000	Water
[21]	90	0.4	60 × 40, 20 × 55								Liquid nitrogen
[11]	∼ 3400	136	1200×100×95	1160 × 70		×			2		Water
[22]	8 − 780	8 − 240	80 × 30 × 40			×					Liquid nitrogen
[12]			50 × 50 × 25		×	×					Liquid nitrogen
[13]	∼ 540	240		∼ 2.5 − 8		×			1 − 5		Liquid nitrogen
[4]	5900−12000		1200 × 100 × 95	4.5 × 3.14		×					–
[18]		1.35		50 − 3		×					Water
[19]			200 × 74 × 3		×				5		Water
[14]		100	500 × 60 × 60								Water/ Liquid nitrogen
[17]			300 × 80 × 60			×			3		Water
[15]	5.2		25 × 34 × 10.5			×	×				Water/ Liquid nitrogen
[16]							×		to 200		–

Figure 1 shows the cross-section dimensions of the mirror. The mirror length is 300 mm. The origin of coordinates was placed in the center of the reflecting surface.

Heat flux was supplied from the top of the mirror, the „heating“ zone, the irradiated zone width was equal to 2 mm. Heat flux density was defined depending on coordinates and corresponded to the Gaussian distribution. Mean heat flux density $q_w = 1$ W/mm^2.

Real monochromator designs use multilayer mirror optics. This study estimated the variability of layer properties in terms of the equivalent thermal conductivity coefficient. The mirror material is silicon [23,24]. Simulation was performed both without and with a copper radiator ($\alpha = $ const and var, respectively). The cooled region (radiator) height was 7 mm, the length was equal to the mirror length. For cooling „without radiator“ the coolant (water) temperature and heat transfer coefficient were defined on the „cooling“ surface. In all cases, conditions of radiant heat exchange with the environment were defined at all other boundaries (vacuum, temperature 25°C, mirror emissivity factor was set to 1). It was considered that cooling was supplied via two independent tubes, therefore a plane-of-symmetry

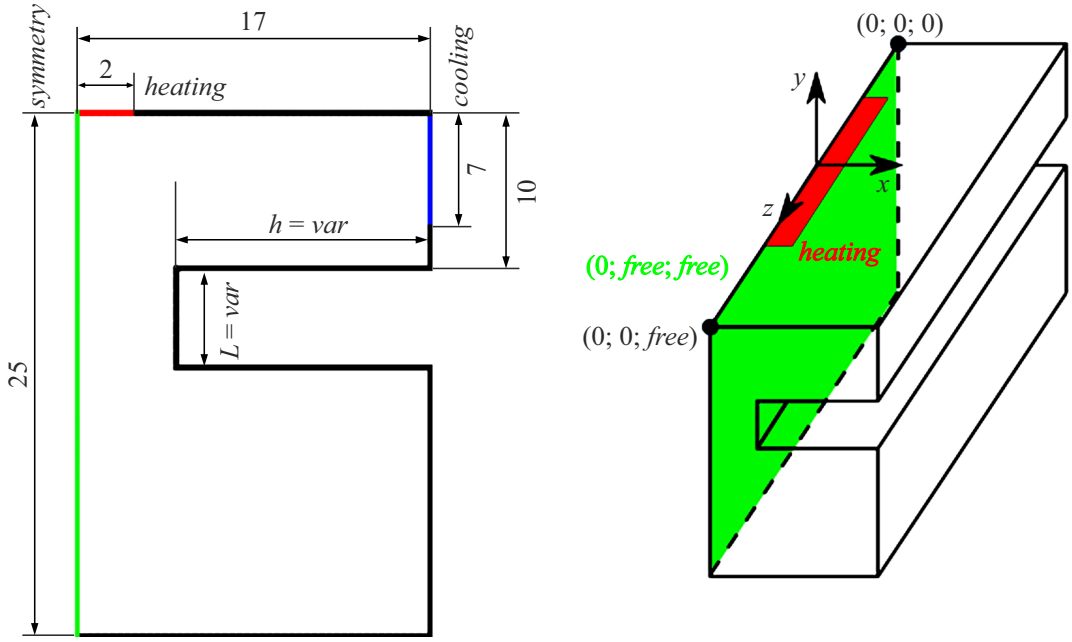

Figure 1. Dimensions of the mirror, mirror attachment method.

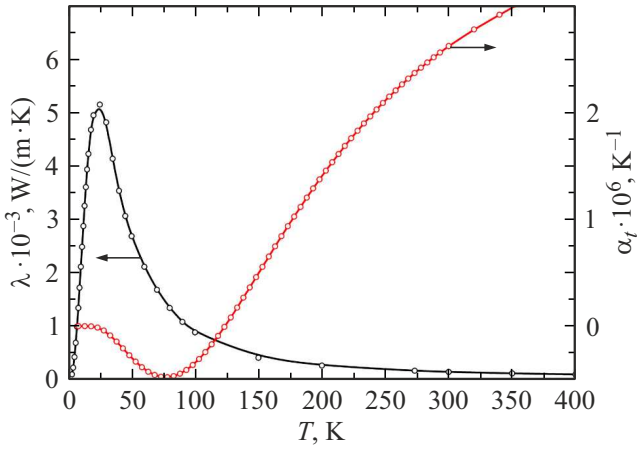

Figure 2. Dependence of the thermal conductivity and thermal expansion coefficients of silicon on temperature.

problem may be considered. A steady-state heat exchange mode was assumed. The thermal conductivity coefficient of silicon was defined as a function of temperature derived after data approximation [24] (Figure 2). The cooling water temperature at the radiator inlet was set to 22°C.

Tabular thermal expansion coefficients were used for thermal strain simulation [23] (Figure 2). The mirror was fixed as follows: the plane of symmetry could not move along the x axis. One of the points on the plane of symmetry was fully fixed and couldn't move along all axes. The second point on the plane of symmetry could move along the z axis.

2. Mathematical problem formulation

A system of equations was solved for evaluation of the thermal strain state:

$$\varepsilon_x = \frac{1}{E}[\sigma_x - \mu(\sigma_y + \sigma_z)], \quad \gamma_{xy} = \frac{1}{G}\tau_{xy},$$
$$\varepsilon_y = \frac{1}{E}[\sigma_y - \mu(\sigma_z + \sigma_x)], \quad \gamma_{yz} = \frac{1}{G}\tau_{yz}, \qquad (1)$$
$$\varepsilon_z = \frac{1}{E}[\sigma_z - \mu(\sigma_y + \sigma_x)], \quad \gamma_{zx} = \frac{1}{G}\tau_{zx},$$

where E and G are the modulus of elasticity and shear modulus, μ, λ are Poison's ratio and Lame constant, with the following dependences between them: $G = \frac{E}{2\cdot(1+\mu)}$, $\lambda = \frac{E\cdot\mu}{(1+\mu)(1-2\cdot\mu)}$, γ is the shear angle, σ, τ are normal and tangential stresses, [Pa].

Total strains were defined as follows:

$$\varepsilon_x = \varepsilon_x^y + \alpha_t \cdot T,$$
$$\varepsilon_y = \varepsilon_y^y + \alpha_t \cdot T, \qquad (2)$$
$$\varepsilon_z = \varepsilon_z^y + \alpha_t \cdot T,$$

where ε_x^y, ε_y^y, ε_z^y are elastic strains, α_t is the thermal expansion coefficient, T is the temperature, [K].

Temperature field was derived by solving the thermal conductivity equation:

$$\frac{\partial}{\partial x}\left(\lambda\frac{\partial T}{\partial x}\right) + \frac{\partial}{\partial y}\left(\lambda\frac{\partial T}{\partial y}\right) + \frac{\partial}{\partial z}\left(\lambda\frac{\partial T}{\partial z}\right) = 0. \qquad (3)$$

Here, x, y, z are Cartesian coordinates, [m], λ is the thermal conductivity coefficient of the mirror material [W/(m·K)].

To consider heat exchange within the copper radiator, a system of Navier-Stokes equations supplemented by k-ω SST turbulence model was additionally solved.

3. Mathematical model test results

Thermal calculations were performed with a double accuracy of computation. For the 'without radiator' case, one energy equation was solved. The solution was converged with an accuracy in the order of 10^{-15}. According to the grid convergence results, a grid with approximately 2 000 000 computational cells was chosen for the thermal problem. Further grid refinement didn't cause any change in the temperature profiles. For radiator cases, as many as 7 differential equations were solved (conservation equation, equation of motion in projections to appropriate axes, energy equation, equation for turbulence kinetic energy and dissipation. The solution was converged with an accuracy not worse than 10^{-6}.

Figure 3 shows the comparison of linear movements of the irradiated surface along the x axis. Three computational grids with different number of elements were studied: 750 000, 1 500 000 and 3 000 000. For all described computational grids, movement data coincided, suggesting that further strength calculations may use grids with 750 000 elements.

4. Thermal calculations. Comparison of simulation results with and without copper radiator

A high heat flux density absorbed by the mirror and small heat flux application area lead to uneven temperature distribution inside a silicon mirror and on its external surface. Figure 4 shows a typical mirror temperature field without a copper radiator: the maximum temperature is observed on top near the plane of symmetry and the minimum temperature is observed at the ends. In this case, α was set to a constant value on the mirror side. For α = var, i.e. for the case with an attached copper radiator, the temperature field is alike.

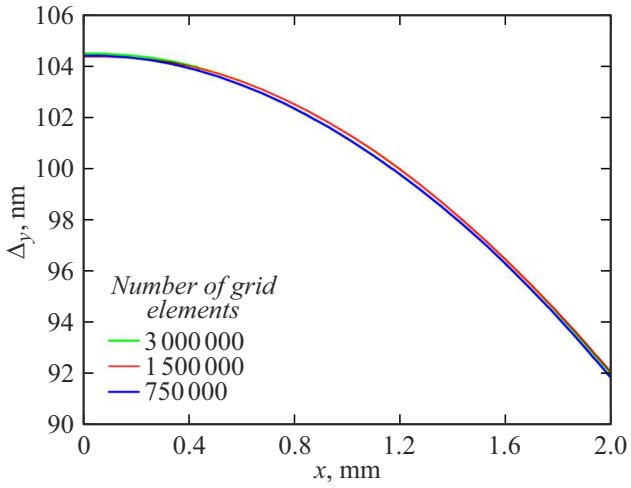

Figure 3. Grid convergence for thermal strain state calculations of a silicon mirror.

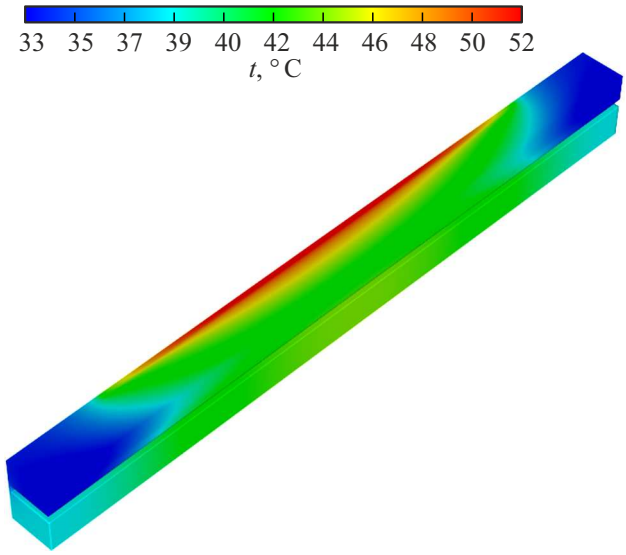

Figure 4. Typical temperature field of the mirror.

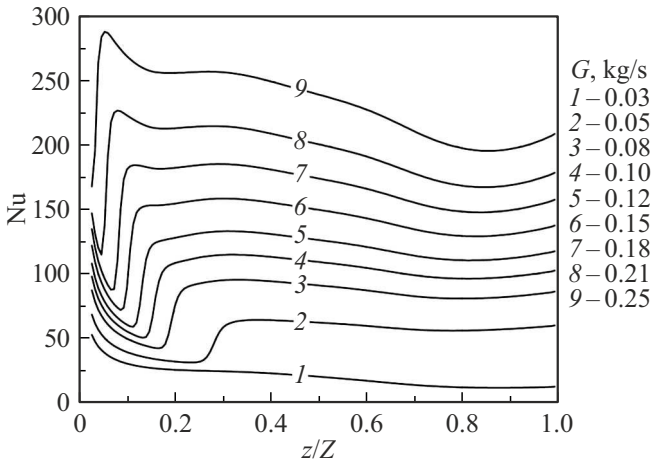

Figure 5. Local Nusselt number variation along the cooling radiator.

Since coolant is heated as it flows within the radiator, the heat transfer coefficient varies lengthwise. Figure 5 shows the local Nusselt number variation along the radiator cooling tube length depending on the coolant mass flow rate. The Nusselt number was calculated from the simulation data as follows:

$$\mathrm{Nu} = \frac{-\lambda\left(\frac{\partial T}{\partial y}\right)_w}{T_w - \overline{T}} \frac{d}{\lambda}, \tag{4}$$

where q, [W/m^2] is the local heat flux, T_w, [K] is the wall cross-section temperature, $\overline{T}$, [K] is the coolant bulk cross-section temperature, d, [m] is the tube diameter, λ,

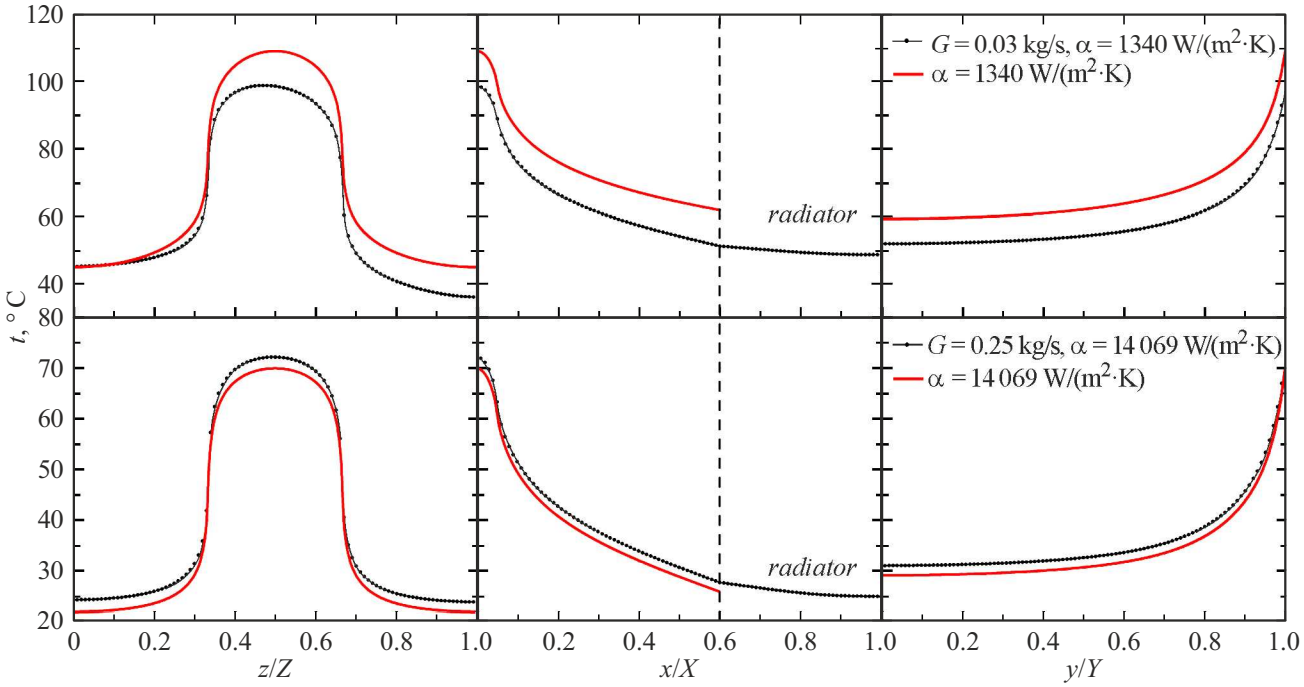

Figure 6. Comparison of the irradiated zone temperature for cooling with a copper radiator (empty dots) and for the case corresponding to a constant heat transfer coefficient equal to the mean heat transfer for the radiator case.

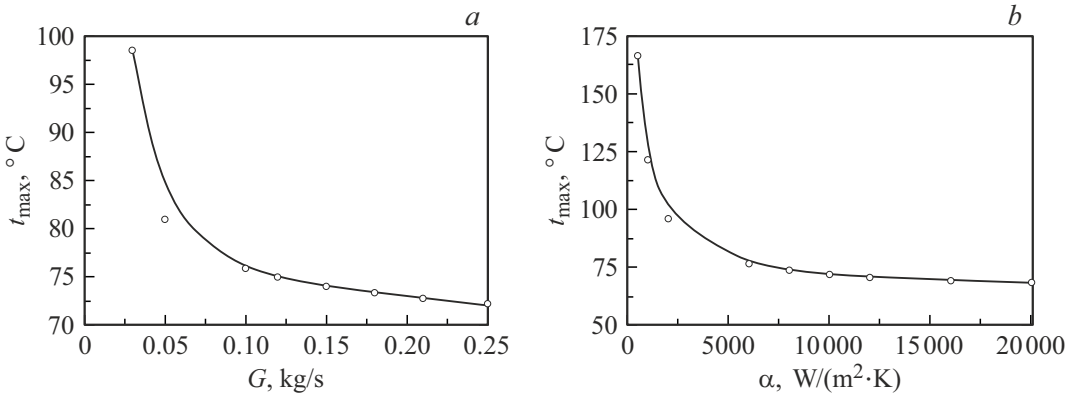

Figure 7. Maximum mirror temperature depending on the coolant flow rate (a) and heat transfer coefficient (b).

[W/(m·K)] is the coolant thermal conductivity coefficient. Almost in all cases, with a relative length $z/Z < 0.3$, there is first a rapid drop and then growth of the Nusselt number, where Z is the radiator mirror length. A further increase in the length causes a smooth decrease in the local Nusselt number. This Nusselt number behavior is associated with the boundary layer growth on the tube walls and further laminar-turbulent transition. Diagram 5 was used to calculate the mean heat transfer coefficient for the side wall that was included in further calculations at $\alpha = \text{const}$. Figure 6 shows comparison of simulation data for $\alpha = \text{var}$ (black circles) and the corresponding mean values of $\alpha = \text{const}$ (red lines). With high values of α ($\alpha > 6000\,\text{W/(m}^2\cdot\text{K)}$) (which is equivalent to a high coolant flow rate), symmetric surface temperature profile distribution is observed. With $\alpha < 6000\,\text{W/(m}^2\cdot\text{K)}$, symmetric temperature profiles were observed only in calculations with $\alpha = \text{const}$, when a radiator is considered, both asymmetric temperature distribution along the mirror and considerable difference in the temperature values are observed (a difference between $\alpha = \text{const}$ and $\alpha = \text{var}$ may be 10 degrees and more). Therefore, when a mirror temperature is estimated with low coolant flow rates, a conjugate problem of heat exchange with cooling radiators shall be solved. At high coolant flow rates (and relevant high values of $\alpha > 6000\,\text{W/(m}^2\cdot\text{K)}$), a mirror temperature may be estimated to the approximation of $\alpha = \text{const}$.

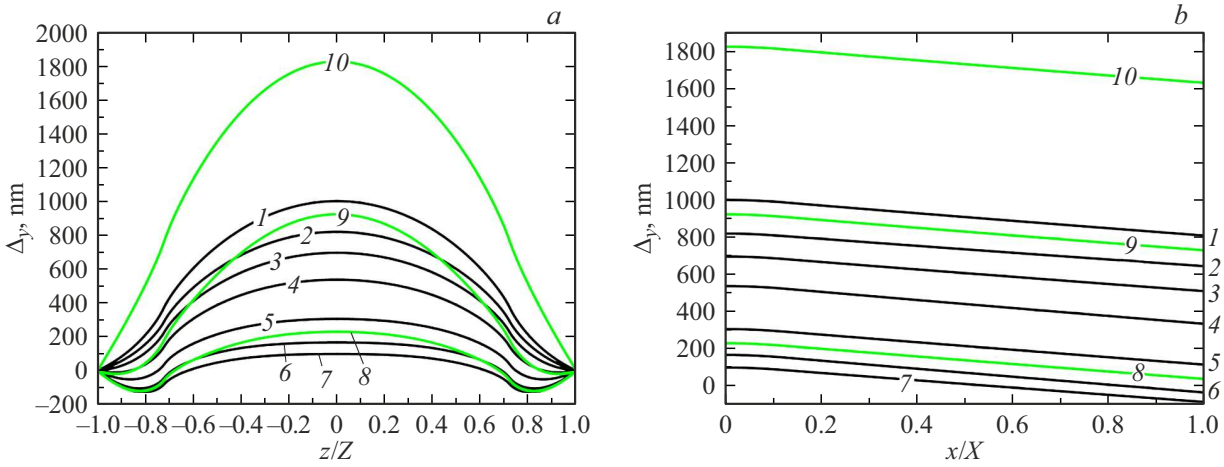

Figure 8. Mirror surface movements along (a) and across (b) the mirror. (h = 0, 2, 4, 6, 8, 10, 12, 14, 16, 17 mm — lines 1–10, respectively).

Figure 7 shows the maximum silicon mirror temperature variation depending on the coolant flow rate (Figure 7, a) and depending on the heat transfer coefficient (Figure 7, b). It is shown that with $\alpha > 6000\,\mathrm{W/(m^2 \cdot K)}$ the maximum mirror temperature almost remains unchanged, this suggests that further increase in the heat transfer coefficient doesn't cause any significant change in the internal mirror temperature field. When the radiator is considered, an increase in the coolant flow rate causes slow reduction of the maximum mirror temperature, which is probably attributed to the radiator effect (heat transfer surface of the radiant component of heat exchange increases). In both cases, with fixed heal load ($q \sim 10^6\,\mathrm{W/m^2}$), the maximum mirror temperature is approximately equal to 75°C.

5. Groove depth effect on the thermally induced mirror surface strain

Section 5 shows the simulation of the thermal strain state of the silicon mirror. The groove depth effect on linear movements is shown in Figure 8. Line *1* represents linear movements along the mirror surface without side grooves. Lines *2*–*9* are strains with an increasing groove depth, *10* — are strains with a fully removed bottom (the groove goes all the way through). In this case, linear strains decrease with the groove depth up to 12 mm and reach their lowest values at 12 mm (the groove height is equal to 3 mm in this case). When the groove depth is larger than 12 mm, an increase in the linear strains is observed. Angular movements (Figure 9) also decrease as the groove depth increases to 12 mm, and then start increasing. (Figure 8 onwards, Z is the mirror length, $X = 17$ mm is the mirror half-width).

Maximum linear and angular movements of the mirror surface depending on the groove depth is shown in Figure 10 (H is the maximum groove depth corresponding to the mirror half-width. With $H = 17$ mm, the mirror

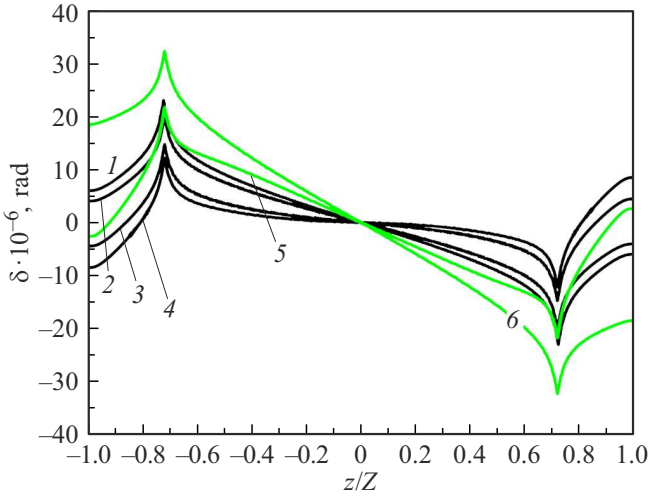

Figure 9. Angular movements along the mirror surface. (h=0, 2, 8, 12, 16, 17 mm — lines 1–6, respectively).

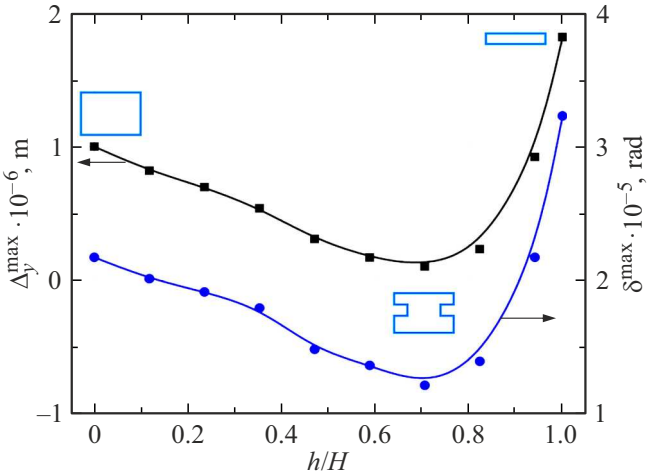

Figure 10. Maximum strains and angular movements depending on the groove depth.

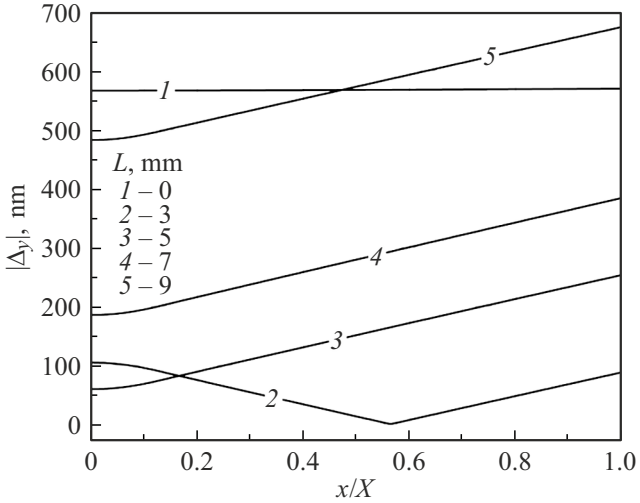

Figure 11. Groove height effect on the absolute strain with a fixed groove depth.

has no bottom at all). Smart-cut provide a decrease in linear strains by almost 10 times, whilst angular movements decrease by approximately 8 times. On all above-mentioned curves, the groove height was fixed and equal to 3 mm.

Groove height also affects the finite thermal strain (Figure 11). Thus, minimum movements across the mirror width are observed with a groove height of 3 mm on average, however, in the irradiated area $x/X < 0.15$, minimum movements are observed when the groove height is 5 mm, whilst the mean absolute movement across the width is higher than that for a groove height of 3 mm.

Conclusion

Numerical simulation of a thermally induced strain state of silicon mirrors of a synchrotron radiation source with a high heat flux density has been performed. Simulation results have shown that:

1. For silicon mirror cooling with a heat transfer coefficient lower than 6000 $W/(m^2 \cdot K)$, the effect of heat transfer coefficient variation along the mirror length shall be considered for evaluation of the temperature field.

2. $\alpha > 6000$ $W/(m^2 \cdot K)$ doesn't cause any significant temperature field variation.

3. Smart-cut may reduce thermally induced linear movements of the mirror by almost an order of magnitude, and angular movements may reduce the movements by almost 8 times. This decrease in linear and angular movement is observed in the given case. When the heat load or mirror material properties change, a new improvement calculation of side grooves shall be carried out because the internal mirror temperature field and relevant strains change.

Acknowledgments

The authors are grateful to D.P. Karasev and A.E. Serdyukov, students of group GS-81 at the aircraft department of Novosibirsk State Technical University, for their participation in calculations.

Conflict of interest

The authors declare no conflict of interest.

References

[1] L.-M. Jin, W.-Q. Zhu, Y. Wang, N.-X. Wang, J.-F. Cao, Z.-M. Xu. Nucl. Instrum. Methods Phys. Research Section A: Accelerators, Spectrometers, Detectors and Associated Equipment, **902**, 190 (2018). DOI: 10.1016/j.nima.2018.06.015

[2] R.L. Headrick, K.W. Smolenski, A. Kazimirov, C. Liu, A.T. Macrander Rev. Scientific Instrum., **73** (3), 1476 (2002). DOI: 10.1063/1.1435819

[3] P. Hu, H. Zhu, C. He. Appl. Thermal Eng., **73** (1), 598 (2014). DOI: 10.1016/j.applthermaleng.2014.07.052

[4] A.M. Khounsary. *SPIE's International Symposium on Optical Science, Engineering, and Instrumentation* (Denver, CO, USA, 1999), p. 10. DOI: 10.1117/12.370114

[5] Y. Li, A. Khounsary, J. Maser, S. Nair. *Proceed. SPIE The International Society for Optical Engineering* (2004), p. 8.

[6] A. Khounsary. J. Maser. Nucl. Instrum. Methods Phys. Research Section A: Accelerators, Spectrometers, Detectors and Associated Equipment, 467–468, 654 (2001). DOI: 10.1016/S0168-9002(01)00438-7

[7] J. Stimson. *Dissertation Submitted for the Degree of Philosophiae Doctor* (PhD), (Birmingham, (2018), p. 265.

[8] G. Maro, M. Rossat, A. Froind, S. Yoksh, H. Kavata, L. Chzhan, E. Tsigler, L. Berman, D. Chapman, J.B. Gastings, M. Iarocci. Rev. Scientific Instrum., **63** (1), 477 (1992). DOI: 10.1063/1.1142736

[9] D. Pauschinger, K. Becker, R. Ludewig. Rev. Scientific Instrum., **66** (2), 2177 (1995). DOI: 10.1063/1.1145697

[10] Y.R. Jaski, M. Meron, P.J. Viccaro. *SPIE's International Symposium on Optical Science, Engineering, and Instrumentation* (San Diego, 1998), p. 62–71. DOI: 10.1117/12.331118

[11] A. Khounsary, W. Yun, I. McNulty, Z. Cai, B. Lai. SPIE Conference on Advances in Mirror Technology for Synchrotron X-Ray and Laser Applications, **3447**, 11 (1998).

[12] P. Marion, L. Zhang, L. Goirand, M. Rossat, K. Martel. *Proc. MEDSI* (Hyogo, Japan, 2006), p. 8.

[13] L. Zhang, M. Sánchez del Río, G. Monaco, C. Detlefs, Th. Roth, A.I. Chumakova, P. Glatzel. J. Synchrotron Rad., **20** (4), 567 (2013). DOI: 10.1107/S0909049513009436

[14] X. Cheng, L. Zhang, C. Morawe, M. Sanchez del Rio. J. Synchrotron Rad., **22** (2), 317 (2015). DOI: 10.1107/S1600577514026009

[15] M.A. Antimonov, A.M. Khounsary, A.R. Sandy, S. Narayanan, G. Navrotski Nucl. Instrum. Methods Phys. Res. Section A: Accelerators, Spectrometers, Detectors and Associated Equipment, **820**, 164 (2016). DOI: 10.1016/j.nima.2016.02.103

[16] B.S. Petukhov, V.A. Alekseev, Yu.A. Zeigarnik, etc., TVT, (in Russian) **23** (6), 1200 (1985).
[17] P. Brumund, J. Reyes-Herrera, Ch. Morawe, Th. Dufrane, H. Isern, Th. Brochard, M. Sánchez del Río, C. Detlefs. J. Synchrotron Rad., **28** (5), 1423 (2021). DOI: 10.1107/S160057752100758X
[18] P. Oberta, V. Áč, J. Hrdý. J. Synchrotron Rad., **15** (1), 8 (2008). DOI: 10.1107/S0909049507044858
[19] H. Kawata, M. Sato, Y. Higashi, H. Yamaoka, J. Synchrotron Rad, **5** (3), 673 (1998). DOI: 10.1107/S0909049597020268
[20] W.K. Lee, P.B. Fernandez, A.M. Khounsary, W. Yun, E.M. Trakhtenberg. *Optical Science, Engineering and Instrumentation '97* (San Diego, 1997), p. 208−215. DOI: 10.1117/12.294480
[21] S. Joksch, G. Marot, A. Freund, M. Krisch. Nucl. Instrum. Methods Phys. Res. Section A: Accelerators, Spectrometers, Detectors and Associated Equipment, **306** (1−2), 386 (1991). DOI: 10.1016/0168-9002(91)90345-Q
[22] A.I. Chumakov, I. Sergeev, J.-Ph. Celse, R. Rüffer, M. Lesourd, L. Zhang, M. Sánchez del Río. J. Synchrotron Rad., **21** (2), 315 (2014). DOI: 10.1107/S1600577513033158
[23] Y.S. Touloukian, R.K. Kirby, R.E. Taylor, T.Y.R. Lee. *Termal expansion. Nonmetallic solids*, **13**. in Thermophysical Properties of Matter, **13**, (1977).
[24] Y.S. Touloukian, R.W. Powell, C.Y. Ho, P.G. Klemens. *Thermophysical properties of matter* (Boston, MA: Springer US, 1970), v. 1. DOI: 10.1007/978-1-4615-9600-4

Translated by E.Ilinskaya